

This item is the archived peer-reviewed author-version of:

Thermal modelling and validation of a direct rotor cooled permanent magnet electric machine

Reference:

Nonneman Jasper, T' Jollyn Ilya, Vanhee Steven, De Paepe Michel.- Thermal modelling and validation of a direct rotor cooled permanent magnet electric machine
IEEE International Electric Machines and Drives Conference (IEMDC), MAY 15-18, 2023, San Francisco, CA - ISBN 979-83-503-9899-1 - New York, IEEE, (2023), p. 1-5
Full text (Publisher's DOI): <https://doi.org/10.1109/IEMDC55163.2023.10238978>
To cite this reference: <https://hdl.handle.net/10067/2003180151162165141>

Thermal Modelling and Validation of a Direct Rotor Cooled Permanent Magnet Electric Machine

Jasper Nonneman^{1,3}, Ilya T’Jollyn^{1,2}, Steven Vanhee⁴, Michel De Paepe^{1,3}

Email: {Jasper.Nonneman,Michel.DePaepe}@UGent.be Ilya.TJollyn@UAntwerpen.be Steven.Vanhee@Dana.com

¹Department of Electromechanical, Systems and Metal Engineering, Ghent University, Sint-Pietersnieuwstraat 41, 9000 Ghent, Belgium

²Department of Electromechanical Engineering, University of Antwerp, Antwerp, Belgium

³Flanders Make@UGent – Core lab MIRO, Belgium

⁴Dana Belgium NV, Ten Briele 3, 8200 Brugge, Belgium

Abstract—A novel direct rotor cooling method for electric machines is proposed and the performance is evaluated based on a thermal zonal model that is validated with measurements on a rotor heater setup. The trend of increasing power density of electric machines urges the need for high performance rotor cooling methods. A thermal model is needed to assess the performance of these methods on a certain geometry and to optimize the design. A previously developed thermal zonal model of an interior permanent magnet synchronous machine is extended with the novel direct rotor cooling method and validated with measurements on a rotor heater setup for different oil inlet temperatures (40 to 80°C), flow rates (0.5 to 10 l/min) and heating powers (261 to 873W). With a maximum absolute and relative deviation between the measurements and simulations of respectively 6.3°C and 13.3% on the maximum rotor core temperatures for flow rates higher than 1 l/min, it is concluded that the model is sufficiently accurate when taking into account the assumptions and uncertainties on the input parameters. A model based comparison with the validated model shows the great potential of the novel direct rotor cooling method to push the power density to higher levels, since the relative magnet temperatures can be decreased by 71% compared to a hollow shaft liquid cooled machine.

Keywords— *Electric machine thermal management, Hollow shaft liquid cooling, Novel direct rotor cooling, Thermal zonal model, Model validation, Rotor heater measurements*

I. INTRODUCTION

With the increasing trend of electrification in the automotive industry, electric drivetrains are pushed to higher power densities to increase the performance and efficiency of the vehicle. A commonly used electric machine in these drivetrains is the Interior Permanent Magnet Synchronous Machine (IPMSM) [1]. The higher power densities are not only a challenge from an electromagnetic perspective, but also regarding thermal management, since excessive temperatures within the components are detrimental. The winding is the most vulnerable component within the stator assembly where the maximum temperature is limited by the wire insulation, which is for example 180°C for an insulation of class H. In addition to the stator winding, a significant amount of heat is generated within the rotor core and permanent magnets. The rotor region is thermally connected to the stator region and housing jacket by convective heat transfer at the end space and airgap, and conductive heat transfer at the bearings, both providing a bad thermal contact. Excessive temperatures of the magnets reduce the remanence and coercivity, resulting in a decreased machine torque and potentially demagnetization. Therefore the temperature in the magnets should be maintained below the maximum allowed temperature, which is for example 180 °C for UH-grade NeFeB magnets [1].

To sufficiently cool the stator, the most commonly used method is jacket cooling at the housing of the machine. More advanced methods to cool the stator windings are direct stator cooling, direct coil cooling and end winding (jet) cooling [2]. Especially for high power density machines where the speed of the machine is pushed to its limits, high frequency losses occur in the rotor and permanent magnets [1]. To avoid excessive temperatures within the rotor at these demanding operating points, an active rotor cooling technique is required. Recently several implementations of rotor cooling have been investigated in scientific literature, where roughly two categories can be found. Within the first category, the heat or coolant is transferred out of the rotor through the shaft. The indirect hollow shaft liquid cooling and rotating heat pipe cooling techniques are examples of this category [2] [3] [4]. For the cooling methods in the second category, a coolant (mostly oil) is provided by the shaft or the end space and cools the external surfaces of the rotor such as spray and jet cooling [4] [5] [6]. In that case, the coolant does not leave the rotor by the shaft, but splashes around in the end space of the machine. A scavenging system is then needed to evacuate the oil from the end space of the machine. With the methods of the first category, the end space is dry such that no additional windage losses are induced by a coolant in the end space or airgap and no scavenging is needed. Hollow shaft liquid cooling is the most conventional method, since it is relatively easy to manufacture and reliable but lacks in thermal performance due to the relatively high interface resistances from heat source (rotor core and magnets) to the coolant within the shaft [3]. To overcome this issue a novel method of the first category is proposed and investigated within this study. In this novel method, coolant channels are introduced within the rotor core on locations where magnetic material can be removed without significant impact on the rotor magnetic field and its core losses. This results in the elimination of thermal interface resistances, a short conductive heat transfer path and a high heat transfer area between coolant and rotor core.

Lumped parameter thermal networks (LPTN) are very attractive for quick predictions, design optimization and parameter sensitivity analysis which make them most suitable to simulate the performance of the direct rotor cooling method and optimize the design [7]. Therefore a previously developed zonal thermal model of an interior permanent magnet machine is extended to include the novel direct rotor cooling method [8]. To validate the implementation of the direct rotor cooling method, the rotor of the machine is experimentally investigated in this study with a rotor heater setup and the measurements are compared to the simulations of each setpoint. With the validated model, a comparison is made between a machine with indirect hollow shaft liquid cooling and the novel method proposed here, direct rotor cooling.

II. MACHINE GEOMETRY WITH THE NOVEL DIRECT ROTOR COOLING METHOD

The electric machine under investigation is an off-the-shelf IPMSM with a V-shaped magnet configuration. A symmetric part of the cross section is shown in Fig. 1. The machine has a stack length of 140 mm and the stator and rotor respectively consist of 48 slots and 8 magnetic poles. The main geometric properties of this machine are shown in TABLE I. The maximum speed and peak torque of the machine are rated at respectively 15000 rpm and 195 Nm, with a maximum output power of 109 kW when the motor is supplied by a DC link voltage of 394 V.

Within this machine, lightening holes are present within the rotor iron close to the permanent magnets. These spaces are used as cooling channels within this study and the shaft and balancing plates of the machine are redesigned to guide the flow through these holes as shown in Fig. 3. The inlet and outlet are located in the shaft at the front of the motor. The oil first flows through an axial centered bore hole to the back of the motor, from where it goes to the back balancing plate collector. It then passes through the rotor channels and is collected in the front balancing plate from where it goes back to the radially spaced axial channels in the shaft through radially drilled passages. A lubrication oil is used as coolant, since there is direct contact with corrosion sensitive components and the oil is already available in an electric vehicle.

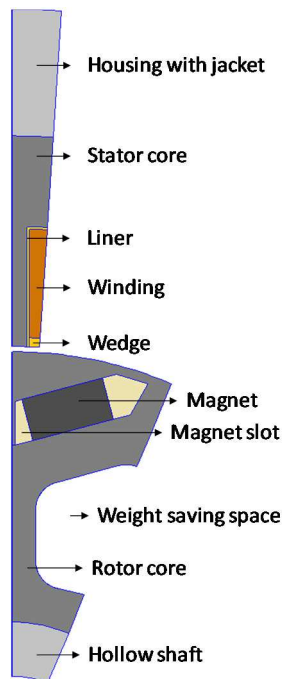


Fig. 1: Machine geometry

TABLE I: MOTOR GEOMETRIC PROPERTIES

Parameter	Value
Shaft diameter	42 mm
Rotor outer diameter	119 mm
Stator inner diameter	120.5 mm
Stator outer diameter	180.5 mm
Housing diameter	216.5 mm

III. MACHINE THERMAL ZONAL MODEL

A previously developed thermal zonal model (ZM) for an electric machine is extended with direct rotor cooling and used within this study. The zonal model is a LPTN that combines the benefits of analytical approaches and finite element modelling (FEM). Axial symmetry in the rotor/stator poles is assumed so only half of a stator and rotor pole is modelled. The equivalent thermal network in the axial direction (perpendicular to the section shown in Fig. 1) and end plates is determined with an analytical approach since they have a uniform cross section and low temperature gradients occur here. In the radial and tangential direction (with the origin in the center of the shaft in Fig. 1) higher temperature gradients occur. The proposed solution is to use a 2D FEM to accurately determine the temperature distribution for the cross section in Fig. 1 and to extract the 2D equivalent thermal resistances from this simulation for a zonal discretization of the geometry. Details on the modelling approach are elaborated in the publications of Nonneman et al. [3] [8] [9]. In the following parts of this section, only the specifications of the implementation of the novel direct rotor cooling method are discussed.

The conductive resistances in the active part of the rotor are extracted from the temperature distribution result of the 2D FEM simulation of the cross section as shown in Fig. 2, where the blue lines indicate the zones that are used to construct the 2D zonal model of the rotor. The geometry of the balancing plates is rather complex (grooves for sealing rings and non-uniform cross sections) and therefore the conductive resistances are determined with the same method as for the rotor. An axisymmetric cross section of the balancing plates is simulated in a 2D FEM. Convective boundary conditions are set at the surfaces in contact with the oil. At the rotor and shaft contact region, equivalent convective boundary conditions are set which are determined from the contact resistances between the components and balancing plate.

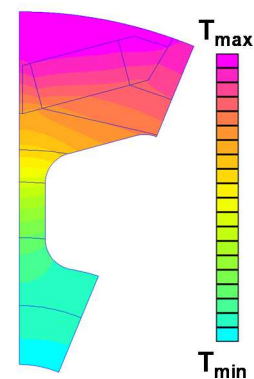


Fig. 2: Rotor zones and 2D FE temperature distribution

The local convective heat transfer in the rotor channels is calculated with a combination of different heat transfer correlations. At standstill, the flow in the channels is both thermally and hydraulically developing due to a combination of relatively short channels and a high Prandtl number of the oil. When the rotor is rotating, it is expected that the convective heat transfer and pressure drop will increase with rotational speed ω due the secondary flow created by the rotating motion and the temperature difference between the boundary layer and the core flow [10]. Further relatively low

flow velocities and according Reynolds numbers (Re) are present in the hollow shaft and direct rotor cooling channels due to the large flow areas, such that free convection can have an important contribution to the heat transfer in the channels [11]. Therefore mixed convection will occur in the channels such that a combination of several correlations is used. In a first step, the effect of the rotation on the heat transfer in case of a fully developed flow is determined with the correlations of Mori et al. [10]. Close to the entrance of the channels, simultaneously developing flow will be dominant. Using the fully developed Nusselt number $Nu_{fd}(\omega)$ with ω the rotational speed, the local Nusselt number Nu_{sd} is calculated with the correlation of Spang et al. [11] for simultaneously developing flow with a constant heat flux boundary condition in the axial direction (1). The latter is a good assumption due to the relatively low thermal conductivity of the stator core in the axial direction due to the laminations.

$$Nu_{sd} = \int_{x_0}^{x_1} \left(Nu_{fd}(\omega)^3 + (1.302(RePrD_h/x)^{1/3})^3 + (0.462 Pr^{1/3}(ReD_h/x)^{0.5})^3 \right)^{1/3} / (x_1 - x_0) \quad (1)$$

In this equation, x is the axial location in the channel, x_0 and x_1 are respectively the beginning and end of the channel section, Pr is the Prandtl number and D_h is the hydraulic diameter. More downstream the heat transfer can be enhanced by free convection. A correction factor was proposed by Petukhov and Polyakov to calculate the Nusselt number Nu_{mx} by local laminar mixed convective heat transfer in a uniformly heated pipe [11]:

$$Nu_{mx} = Nu_{sd} \int_{x_0}^{x_1} ((1 + (Ra^*/B)^4)^{0.045}) / (x_1 - x_0) \quad (2)$$

Where $Ra^* = g\beta\rho^2 D_h^4 q'' Pr / \mu^2 k$ is the modified Rayleigh number, $B = 5 \times 10^3 x^{*-1}$ for $x^* < 1.7 \times 10^{-3}$ and $B = 1.8 \times 10^4 + 55x^{*-1.7}$ for $x^* \geq 1.7 \times 10^{-3}$, q'' is the heat flux, β , ρ , μ and k are respectively the thermal expansion coefficient, density, dynamic viscosity and thermal conductivity of the coolant and $x^* = x/D_h RePr$ is the dimensionless axial location in the channel. The convection coefficient h in a channel section is then calculated from the Nusselt number by simultaneously developing mixed convection Nu_{mx} . For the heat transfer coefficient in the balancing plates channels, the minimum value of the heat transfer coefficient in the hollow shaft channel is used.

IV. EXPERIMENTAL SETUP

To validate the proposed model, a rotor heater setup was constructed which consists of an assembly of the stationary shaft, rotor core, magnets and balancing plates as shown in Fig. 3. An aluminum sleeve with cartridge heaters surrounding the rotor core is used to emulate the hysteresis and eddy-currents losses in the rotor core and magnets which are mostly induced close to the airgap [1]. 16 cartridge heaters of in total maximum 1kW are inserted in 8 drilled holes and supplied by an EA-PS 9072-170 power supply. Oil is provided from an oil conditioning circuit at the desired inlet temperatures T_{in} and flow rates \dot{V} . After the test section the flow rate is measured by one of two Krohne Optimass coriolis flow meters, one for the low flow range (6000FS08) and one for the high flow range (6000FS15). The oil temperature before and after the test section is accurately measured with 1.5mm T-type mineral insulated thermocouples downstream from a twisted tape insert flow mixer ensuring a uniform temperature profile. The temperature of the rotor core is measured at several locations as shown in Fig. 3. K-type mineral insulated thermocouples of 0.5mm are placed in the rotor core between the channels T_{RI} and in the channels to measure the oil temperature T_C . Ultra-fine wire PFA K-type thermocouples are glued into grooves in the active rotor outer surface $T_{ROactive}$, on the edge between the rotor outer surface and balancing plates T_{ROend} and onto the aluminium sleeve T_S . An overview of the range and accuracy of the sensors is shown in TABLE II and more details of the experimental investigation can be found in [12].

TABLE II: SENSORS AND ACCURACY

Sensor	Range	Accuracy (\pm)
K-type TC	20..150°C	0.1°C
T-type TC	20..120°C	0.08°C
Current	0..170A	0.17A
Voltage	0..72V	0.14 V
Flow meters	0..5 l/min 5..30 l/min	7.5 ml/min and $\pm 0.1\%$ 35 ml/min and $\pm 0.1\%$

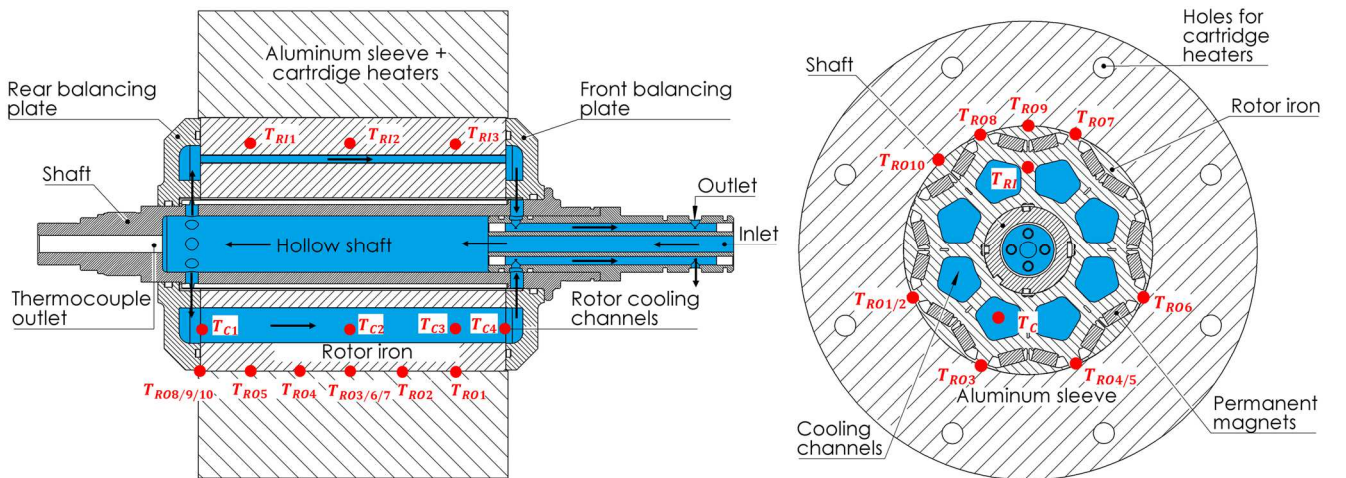


Fig. 3: Rotor heater setup with direct rotor cooling

V. MODEL VALIDATION AND THERMAL PERFORMANCE

A total of 47 steady-state measurements points were made in different ranges of inlet temperature (40 to 80 °C), flow rate (0.5 to 10 l/min) and heating power 261 to 873 W). Within the simulations, the aluminum sleeve and contact resistance with the rotor core are modelled as a convective boundary condition. The contact resistance is estimated from the measurements ($R_{contact} = 645 \text{ mm}^2\text{K/W}$) and the sleeve temperature is iteratively determined until the total convective heat transfer matched the measurement losses. All material properties and boundary conditions that are used within the simulations are shown in respectively TABLE III and TABLE IV. The comparison between the simulations and experiments is shown in Fig. 4, where the temperatures of the simulations and experiments subtracted by the inlet temperature are respectively on the x and y-axis and the green line indicates a perfect match. It is seen that the general trends of all measurement locations are followed relatively well, except for the oil temperature in the channels which is generally lower in the measurement than the simulation. This is caused by the assumption that the oil temperature is uniform in the channel cross section, while it is not the case in the measurement and the measured temperatures are an underestimation of the actual average oil temperatures. The maximum temperature of the rotor core always occurs on the outer surface in the active region $T_{RO_{active}}$. The maximum absolute $\Delta T = T_{sim} - T_{exp}$ and relative temperature deviation $\delta T = \Delta T / (T_{sim} - T_{in})$ in this region are respectively -13.3% and -6.3% for a flow rate higher than 1 l/min . The relative temperature deviations at the edge $\delta T_{RO_{end}}$ and within the rotor core δT_{RI} can get a bit higher due to the smaller temperature difference with the coolant T_{in} . Taking into account the uncertainty on the convective heat transfer correlations, thermal properties of the components and contact resistances, these deviations are acceptable [9].

TABLE III: MATERIAL THERMAL CONDUCTIVITIES (R-RADIAL, T-TANGENTIAL AND A-AXIAL DIRECTION)

Material	k [W/mK]
Housing, flange and balancing plate	210
Stator and rotor core [13]	21.9 (r/t) 1.8 (a)
Permanent magnets [14]	10.2
Permanent magnet slot potting [15]	0.21
Shaft	46.6
Liner and wedge	0.14
Impregnation [15]	0.21
Winding (based on fill factor of 47%) [15]	0.583 (r/t) 181.1 (a)

TABLE IV: CONTACT AND INTERFACE RESISTANCES

Property	Value
Bearing equivalent airgap thickness [16]	0.35 mm
Housing – stator yoke [16]	1321 $\text{mm}^2\text{K/W}$
Shaft – rotor back iron [16]	1321 $\text{mm}^2\text{K/W}$
Housing – flange [16]	1321 $\text{mm}^2\text{K/W}$
Stator core – liner [17]	608 $\text{mm}^2\text{K/W}$
Winding – liner [17]	1799 $\text{mm}^2\text{K/W}$
Permanent magnet – rotor iron [18]	857 $\text{mm}^2\text{K/W}$
Airgap heat transfer coefficient (at 15000rpm) [5]	104.5 $\text{W/m}^2\text{K}$

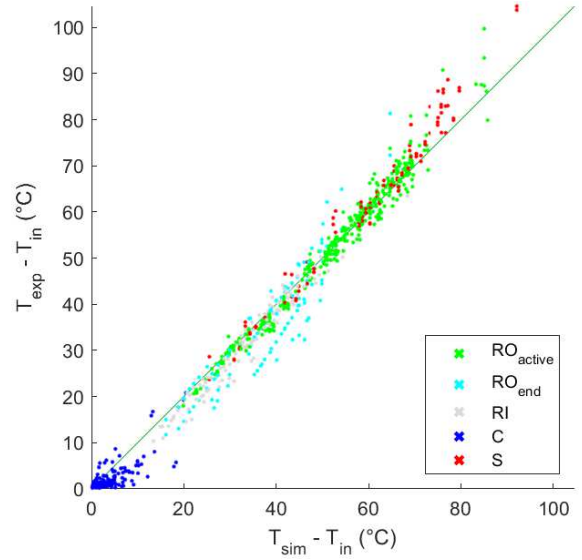


Fig. 4: Direct rotor cooling model validation

To verify the performance of the direct rotor cooling method compared to a standard hollow shaft cooling method, a continuous operating point is selected at 15000 rpm and at a rated torque output of 30 Nm, which resembles the electric vehicle driving at continuous top speed and power. This operating point is the most interesting, since the highest losses are generated in the rotor core and permanent magnets, for which the cooling method is required. The software package Syr-e [19] was used to model the electromagnetic aspects and losses generated in the machine, where the AC losses of the simulated loss maps are rescaled based on the difference with the available total loss map from the manufacturer. The used losses are shown in TABLE V. These losses are distributed uniformly over the volume of the components. Within the comparison a circumferential jacket cooling with water-glycol at 40°C is present in the housing and an oil flow rate of 10 l/min is used at an inlet temperature of 60°C for the hollow shaft and direct rotor cooling. When using hollow shaft cooling only, the maximum magnet temperature is $T_{pm,hstc} = 166.9^\circ\text{C}$, which is close to the maximum temperature of 180°C for UH grade magnets. When adding the direct rotor cooling method, the maximum temperature is reduced to $T_{pm,drc} = 90.7^\circ\text{C}$, which is a relative decrease of 71% on the temperature difference between magnets and coolant $(T_{pm,drc} - T_{pm,hstc}) / (T_{pm,hstc} - T_{in})$.

TABLE V: MACHINE LOSSES AT HIGH SPEED

Parameter	Value
Winding	937.4 W
Stator core	5303 W
Rotor core	434.9 W
Permanent magnets	55.4 W
Airgap	156.1 W
Bearing	146.3 W

VI. CONCLUSIONS

A novel direct rotor cooling method is proposed and investigated which has the potential of increasing the power density of electric machines. A previously developed zonal model is extended with the novel direct rotor cooling method and measurements are performed on a stationary rotor heater setup to validate the implementation of the rotor and cooling method. Measurements are performed at inlet temperatures

from 40 to 80 °C, flow rates from 0.5 to 10 l/min and heating powers from 261 to 873 W. A comparison between the simulated and measured temperatures shows similar trends and a maximum absolute and relative deviation of respectively -6.3°C and -13.3% is determined on the maximum rotor core temperatures for flow rates higher than 1 l/min. To verify the thermal performance of the novel direct rotor cooling method, a comparison is made with a standard hollow shaft liquid cooling method at a high speed continuous operating point. These results show a decrease in temperature difference between the magnets and rotor coolant by 71%, which shows the potential of the novel direct rotor cooling method to push electric machines to higher levels of power density.

ACKNOWLEDGMENT

The author would like to acknowledge Dana Incorporated for supporting this research work.

REFERENCES

- [1] Y. Yang, B. Bilgin, M. Kasprzak, S. Nalakath, H. Sadek, M. Preindl, *et al.*, "Thermal management of electric machines," *IET Electrical Systems in Transportation*, vol. 7, pp. 104-116, 2017.
- [2] Y. Gai, M. Kimiabeigi, Y. C. Chong, J. D. Widmer, X. Deng, M. Popescu, *et al.*, "Cooling of automotive traction motors: schemes, examples, and computation methods," *IEEE Transactions on Industrial Electronics*, vol. 66, pp. 1681-1692, 2018.
- [3] J. Nonneman, B. Van der Sijpe, I. T'Jollyn, S. Vanhee, J. Druant, and M. De Paepe, "Evaluation of High Performance Rotor Cooling Techniques for Permanent Magnet Electric Motors," in *2021 IEEE International Electric Machines & Drives Conference (IEMDC)*, 2021, pp. 1-7.
- [4] X. Wang, B. Li, D. Gerada, K. Huang, I. Stone, S. Worrall, *et al.*, "A critical review on thermal management technologies for motors in electric cars," *Applied Thermal Engineering*, vol. 201, p. 117758, 2022.
- [5] P. O. Gronwald and T. A. Kern, "Traction Motor Cooling Systems: A Literature Review and Comparative Study," *IEEE Transactions on Transportation Electrification*, vol. 7, pp. 2892-2913, 2021.
- [6] R. Wrobel, "A technology overview of thermal management of integrated motor drives-Electrical Machines," *Thermal Science and Engineering Progress*, vol. 29, p. 101222, 2022.
- [7] S. Khalesidoost, J. Faiz, and E. Mazaheri - Tehrani, "An overview of thermal modelling techniques for permanent magnet machines," *IET Science, Measurement & Technology*, vol. 16, pp. 219-241, 2022.
- [8] J. Nonneman, I. T'Jollyn, P. Sergeant, and M. De Paepe, "Quality Assessment of a 2D FE Based Lumped Parameter Electric Motor Thermal Model Using 3D FE Models," in *2020 International Conference on Electrical Machines (ICEM)*, 2020, pp. 973-980.
- [9] J. Nonneman, T. Schoonjans, I. T'Jollyn, A. Selema, R. Sprangers, and M. De Paepe, "Thermal Property Determination of Different Electric Machine Wire Types by Model Variable Fitting on Measurements," in *2022 International Conference on Electrical Machines (ICEM)*, 2022, pp. 1383-1389.
- [10] Y. Mori and W. Nakayama, "Forced convective heat transfer in a straight pipe rotating around a parallel axis:(1st report, laminar regionit)," *International Journal of Heat and Mass Transfer*, vol. 10, pp. 1179-1194, 1967.
- [11] G. Hewitt and J. Barbosa, *Heat exchanger design handbook* vol. 98: Begell house Danbury, CT, 2008.
- [12] J. Nonneman, I. Evans, S. Vanhee, I. T'Jollyn, and M. De Paepe, "Experimental Investigation of a Novel Direct Rotor Cooling Method for an Interior Permanent Magnet Synchronous Machine," in *2022 28th International Workshop on Thermal Investigations of ICs and Systems (THERMINIC)*, 2022, pp. 1-5.
- [13] J. E. Cousineau, K. Bennion, D. DeVoto, and S. Narumanchi, "Experimental characterization and modeling of thermal resistance of electric machine lamination stacks," *International Journal of Heat and Mass Transfer*, vol. 129, pp. 152-159, 2019.
- [14] Y. M. Rabinovich, V. Sergeev, A. Maystrenko, V. Kulakovskiy, S. Szymura, and H. Bala, "Physical and mechanical properties of sintered NdFeB type permanent magnets," *Intermetallics*, vol. 4, pp. 641-645, 1996.
- [15] L. Siesing, A. Reinap, and M. Andersson, "Thermal properties on high fill factor electrical windings: Infiltrated vs non infiltrated," in *2014 International Conference on Electrical Machines (ICEM)*, 2014, pp. 2218-2223.
- [16] D. Staton, A. Boglietti, and A. Cavagnino, "Solving the more difficult aspects of electric motor thermal analysis in small and medium size industrial induction motors," *IEEE Transactions on Energy conversion*, vol. 20, pp. 620-628, 2005.
- [17] S. Sequeira, K. Bennion, J. E. Cousineau, S. Narumanchi, G. Moreno, S. Kumar, *et al.*, "Validation and Parametric Investigations of an Internal Permanent Magnet Motor Using a Lumped Parameter Thermal Model," *Journal of Electronic Packaging*, vol. 144, p. 021114, 2022.
- [18] X. Cai, M. Cheng, S. Zhu, and J. Zhang, "Thermal modeling of flux-switching permanent-magnet machines considering anisotropic conductivity and thermal contact resistance," *IEEE Transactions on Industrial Electronics*, vol. 63, pp. 3355-3365, 2016.
- [19] S. Ferrari, P. Ragazzo, G. Dilevrano, and G. Pellegrino, "Flux-Map Based FEA Evaluation of Synchronous Machine Efficiency Maps," in *2021 IEEE Workshop on Electrical Machines Design, Control and Diagnosis (WEMDCD)*, 2021, pp. 76-81.